# NUCLEATION AND SPINODAL DECOMPOSITION IN TERNARY-COMPONENT ALLOYS

COLLEEN ACKERMANN AND WILL HARDESTY

Abstract. The Cahn-Morral System has often been used to model the dynamics of phase separation in multi-component alloys on large domains. In this paper we examine phase separation on small one-dimensional domains time independently. In particular we use AUTO to create bifurcation diagrams of equilibrium solutions for two different nonlinearities and use Matlab to observe the structure of the material at various points on the diagrams. We compare the results to determine if using different nonlinearities significantly affects the behavior of the Cahn-Morral System.

*Date*: July 30, 2009.
Dr. Thomas Wanner and Dr. Evelyn Sander.

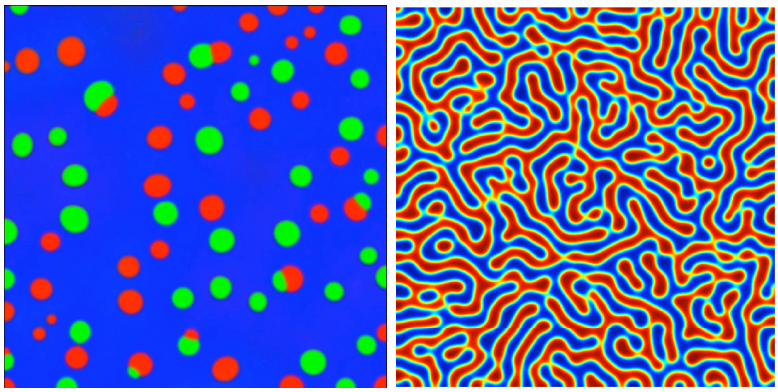

FIGURE 1. The processes of nucleation and spinodal decomposition on two dimensional domains are depicted in these plots. The left plot is an example of a nucleation pattern and the right plot demonstrates spinodal decomposition

## 1. INTRODUCTION

Alloys are composite materials which are formed by mixing a number of pure metals together at a high temperature and then rapidly *quenching* or cooling the mixture to form a solid. During the process of quenching, the components undergo a phase separation in which they begin to form patterns. These pattern formations can be divided into two classes: *nucleation* and *spinodal decomposition*. Qualitatively nucleation occurs when the individual components begin to materialize from the homogeneous mixture as isolated droplets or *droplets*. Spinodal decomposition occurs when the components form connected snakelike patterns. This behavior is modelled mathematically by the Cahn-Morral system.

## 2. BACKGROUND AND RESEARCH METHODS

### 2.1. **Cahn-Morral system.**

The Cahn-Morral system is given by,

$$\begin{aligned} \vec{u}_t &= -\Delta(\varepsilon^2 \Delta \vec{u} + f(\vec{u})) \quad \text{on} \quad \Omega \\ \frac{\partial \vec{u}}{\partial \nu} &= \frac{\partial \Delta \vec{u}}{\partial \nu} = 0 \quad \text{on} \quad \partial\Omega \end{aligned} \tag{1}$$

where $\vec{u} \in \mathbb{R}^3$. The energy of the system is modelled by the Van der Waals free energy functional,

$$E_\varepsilon[\vec{u}] = \int_\Omega \left( \frac{\varepsilon^2}{2} \cdot |\nabla \vec{u}|^2 + F(\vec{u}) \right) dx$$

where $\vec{u} \in \mathbb{R}^3$. The term $-f$ is defined as the derivative of the double-well potential, $F$ from the free energy functional. The domain $\Omega \subset \mathbb{R} = [0, 1]$, has Neumann boundary conditions imposed on the edges where $F : \mathbb{R}^3 \to \mathbb{R}$ and $f : \mathbb{R}^3 \to \mathbb{R}^3$

2.2. **Gibbs Simplex.** The Gibbs simplex is defined as:

$$\mathcal{G} = \{(u, v, w) \in \mathbb{R}^3 \, : \, u + v + w = 1 \, , u \geq 0 \, , v \geq 0 \, , w \geq 0\}.$$

where $\vec{u} \in \mathcal{G} \, \forall \, t$. The Gibbs simplex also represents the set of all possible states or average mass concentrations of the ternary alloy, which follows from the conservation of mass. $\mathcal{G}$ can be divided into regions corresponding to nucleation and spinodal decomposition, which are determined through linearization analysis.

Given a state $(\bar{u}, \bar{v}, \bar{w}) \in \mathcal{G}$, the stability of that particular state is given by computing the eigenvalues of $J_f(\bar{u}, \bar{v}, \bar{w})$, where $J_f$ is the Jacobian of $f(u)$ [4]. The state $(\bar{u}, \bar{v}, \bar{w})$ is in the nucleation region if $J_f$ has no positive eigenvalues. Otherwise it lies in the spinodal region [2]. These regions can be depicted graphically with the Gibbs Triangle, where each color represents a different region.

2.3. **The nonlinearities.** In our research we used two nonlinearities; a quadratic nonlinearity:

$$F(u, v, w) = \frac{u^2 v^2 + (u^2 + v^2)(w^2)}{4}$$

and a logarithmic nonlinearity:

$$F(u, v, w) = 3.5(uv + uw + vw) + u \ln u + v \ln v + w \ln w.$$

The nonlinearities were chosen so that they were triple well potentials and symmetric. Symmetric means that each component contributes to the nonlinearity in the same way, making investigations simpler.

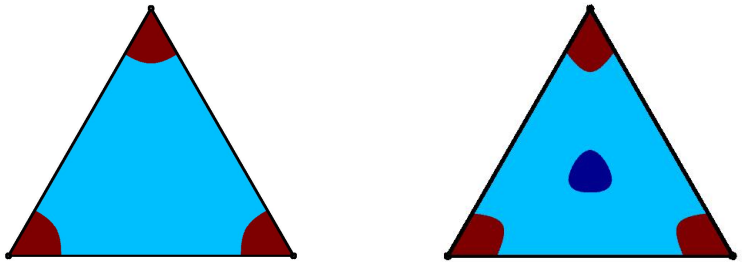

FIGURE 2. The Gibbs triangle for the quadratic nonlinearity is shown on the left, and the triangle for the logarithmic nonlinearity is depicted on the right

Both of the nonlinearities have been investigated previously in both the one and two dimensional cases [3],[4],[2]. However, most of the previous research was done with time variation. Our research differs in that we are looking at solutions at one moment in time and comparing results from different nonlinearities. Also in our case we are using much smaller domains so that we can study the behavior of individual droplets. This differs from past research which dealt with studying the behaviour of groups of droplets on much larger domains.

## 3. Results and Discussion

3.1. **Gibbs Triangle.** For each of our nonlinearities we created Matlab code which shows which regions on the Gibbs simplex have zero, one or two positive eigenvalues. In the pictures below the Gibbs simplex is projected onto the plane.

The red area represents the nucleation region where there are no positive eigenvalues. The light blue and dark blue represent the regions where there are one and two positive eigenvalues respectively, these two areas are considered part of the spinodal region.

3.2. **Path following.** Our ultimate goal in path following was to trace paths in the parameter space of the nucleation region. However, the nontrivial branches of equilibria in the nucleation region are not connected to the trivial branch. To reach the non-trivial nucleation branches we had to begin in the spinodal region.

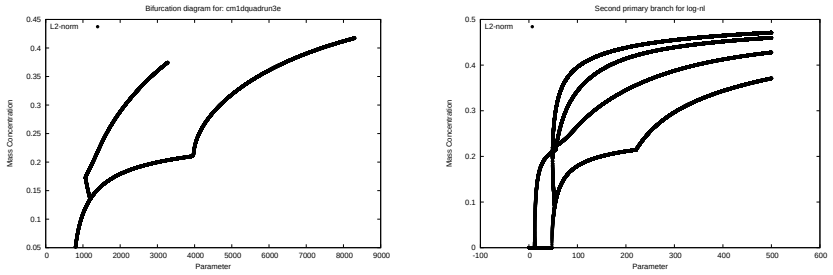


FIGURE 3. This figure displays the bifurcation diagrams for the $\lambda$ runs along the second primary branch for both nonlinearities. The diagram for the quadratic nonlinearity is depicted on the left and the logarithmic nonlinearity is shown on the right

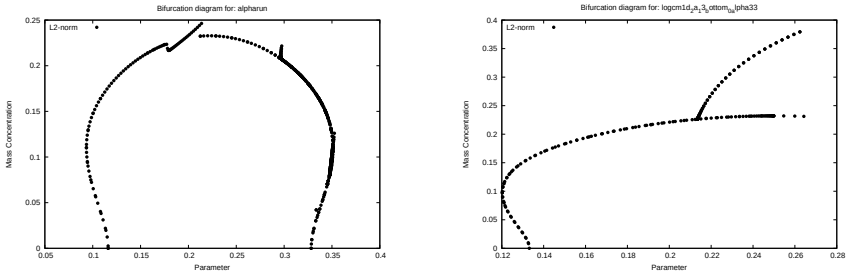


FIGURE 4. This figure compares the alpha runs from both nonlinearities; the plot on the left is from the quadratic nonlinearity and the plot on the right is from the logarithmic nonlinearity

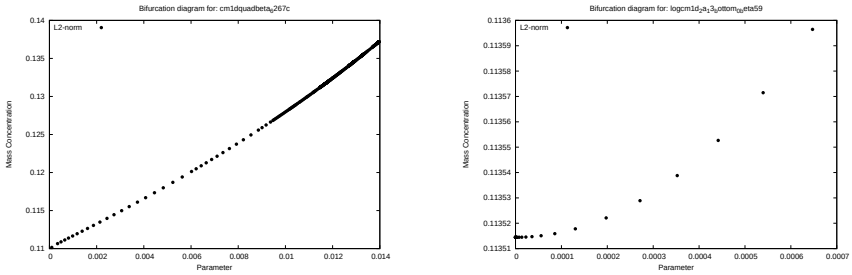


FIGURE 5. This figure compares two successful $\beta$ runs from inside the nucleation region for both nonlinearities; the plot on the left depicts the $\beta$ run for the quadratic nonlinearity where $\lambda = 8000$, $\alpha \approx 0.09344$ and the plot on the right shows the $\beta$ run for the logarithmic nonlinearity with $\lambda = 450$ and $\alpha \approx 0.121$.

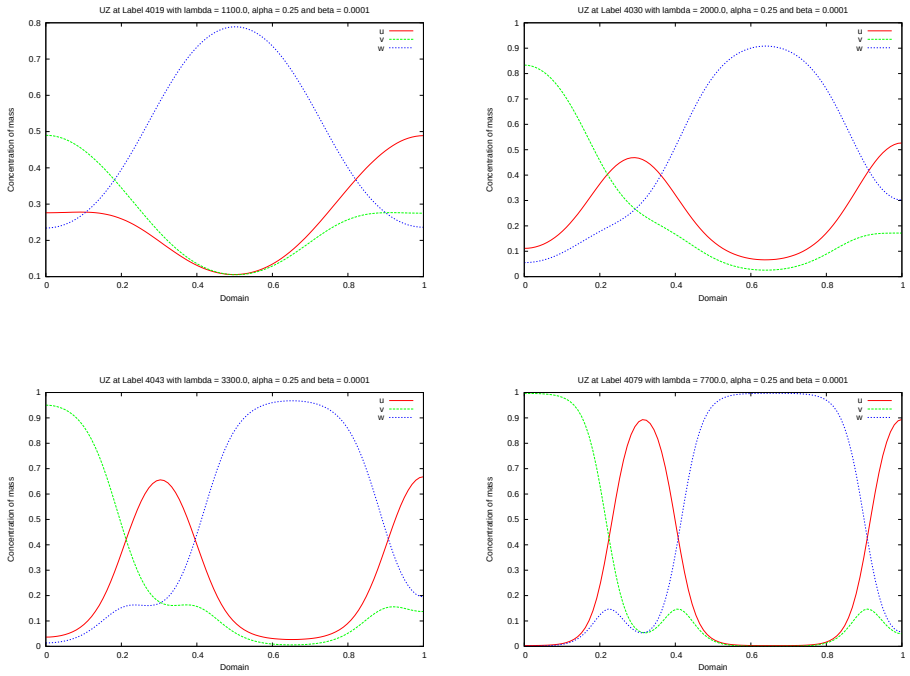


FIGURE 6. This figure depicts the change in droplet formation for the quadratic nonlinearity, as $\lambda$ increases along the secondary branch of figure 3.

This is due to the fact that since the nucleation region is *stable*, it isn't possible to branch out. First we varied $\lambda = 1/\varepsilon^2$. To get onto the second primary branch in the spinodal region. After following the second primary branch and its bifurcations we attempted to follow in $\alpha = (\bar{u} + \bar{v})/2$ back into the nucleation region. Finally we varied $\beta = (\bar{u} - \bar{v})/2$ in the nucleation region.

We were interested in the second primary branch since symmetry of the solutions along that branch ensured that we could get centralized bubble formations. The primary branches occur at the points $\lambda = (n\pi)^2/\mu$ where $n \in \mathbb{N}$ and $\mu$ is the positive eigenvalue of $J_f(u)$. The goal was to follow this branch to a sufficiently large value of $\lambda$ so that when that value is fixed and $\alpha$ is varied back from the primary branch and / or any secondary branch that it will become small enough to reach the nucleation region.

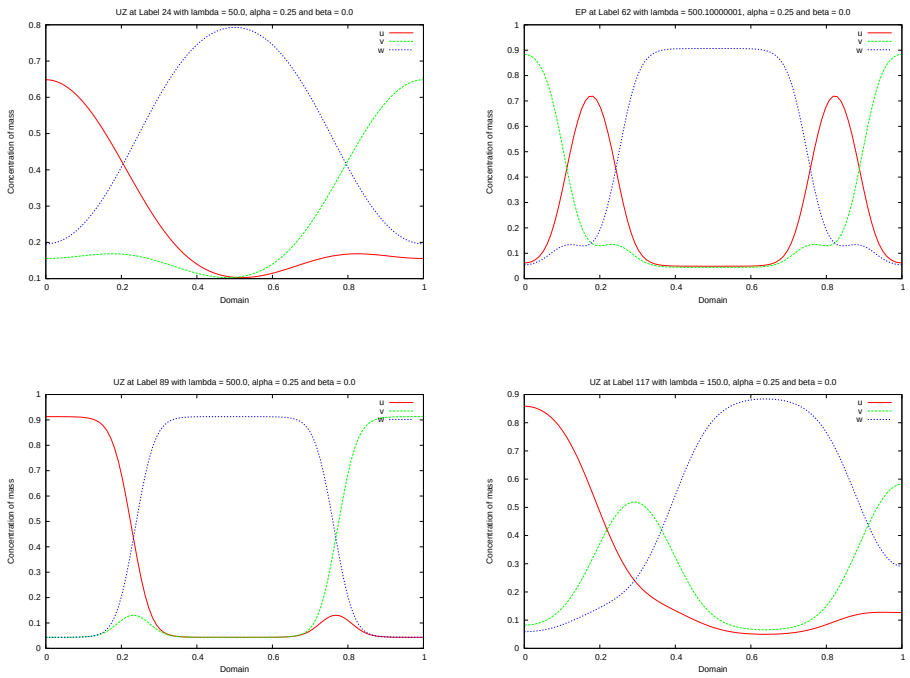


FIGURE 7. This figure depicts the change in droplet formation for the logarithmic nonlinearity, as $\lambda$ increases along the secondary branch of figure 3.

As shown in figure 3, the primary branch for the quadratic nonlinearity was followed out to $\lambda \approx 8000$ where only one secondary branch was detected by AUTO. To reach the nucleation region the $\lambda$ value was fixed at 8000, where the $\alpha$ run originating from the secondary branch reached sufficiently small values. Unfortunately, the $\alpha$ run originating from the primary branch was unable to reach a small enough value to enter the nucleation region. The $\alpha$ run which did enter the nucleation region produced several points from which a $\beta$ varying simulation could be run; it turned out that all but one of these points resulted in spurious runs. The plot on the left in Figure 5 displays the bifurcation diagram produced from the aforementioned $\beta$ run.

For the logarithmic nonlinearity, the first nontrivial branch was easy to find and there were also several bifurcations originating from it. However, the droplet

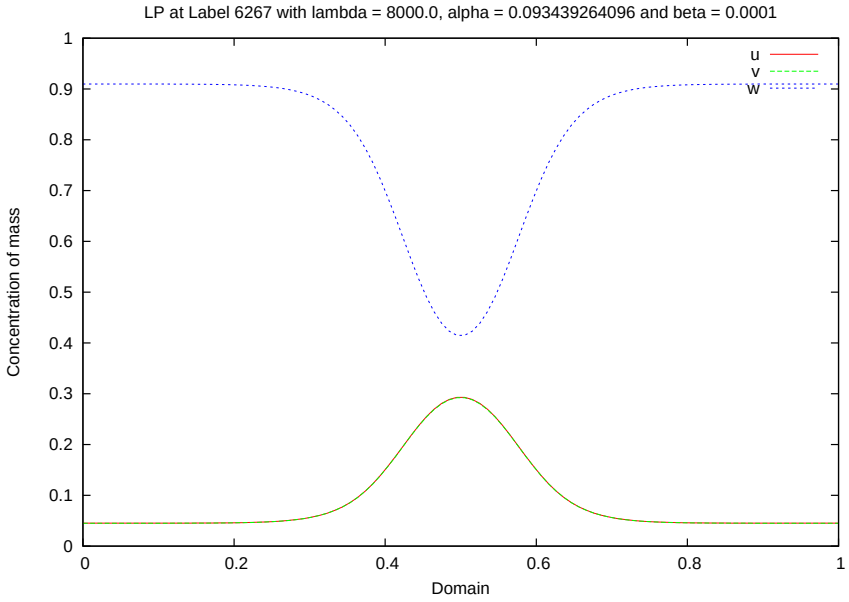


FIGURE 8. This figure depicts the droplet formation occurring at the label from which the $\beta$ run for the quadratic nonlinearity depicted in figure 5 originates.

diagrams were not very interesting, because the average concentration of the u and v components were always exactly the same. Changing $\beta$ from 0 to 0.001 yielded double and single edge droplets, since the $\bar{u}$ and $\bar{v}$ concentrations were different.

The second branch was much more difficult to get onto than the first branch. We could not get onto the second branch with either $\beta = 0$ or $\beta = 0.001$. Therefore we decided to try forcing the symmetry by setting $v(x) = u(1 - x)$, which reduced the complexity of the problem by eliminating a component from the vector $\vec{u}$. This allowed us to add more modes to the discrete cosine transform in our spectral code without using significantly more computing power, which in theory should have increased the accuracy of our results. Unfortunately when using the new symmetric code the second branch still did not appear.

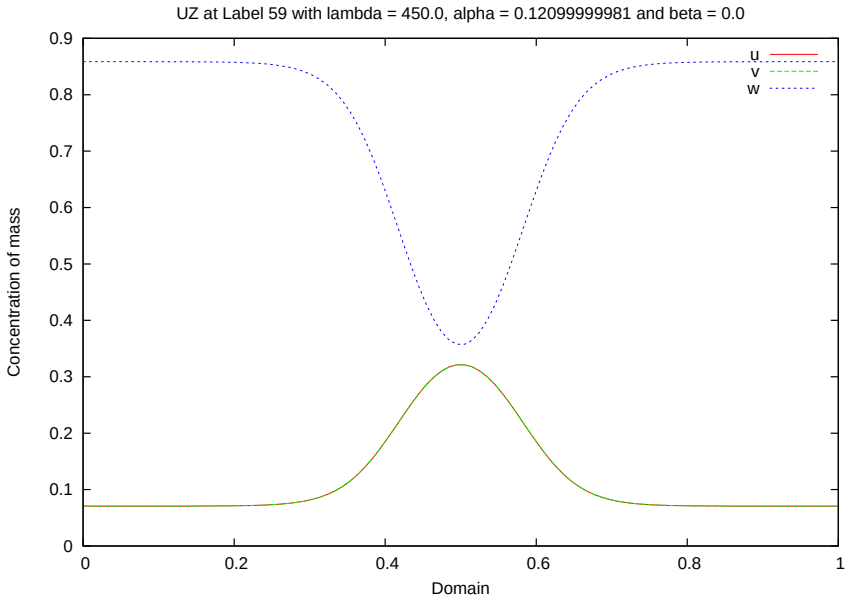


FIGURE 9. This figure depicts the droplet formation occurring at the label from which the $\beta$ run for the logarithmic nonlinearity, depicted in figure 5 originates.

We then changed the step size from $1 \times 10^{-8}$ to $1 \times 10^{-4}$ and the symmetric code was able to go onto the second branch. To determine if the symmetric code played any part in the transition to the second branch we tried using our original code again with the new step size. Once again we successfully moved onto the second branch. This probably worked because now AUTO was getting far enough onto the second branch in the first step that it would not accidentally converge to the original branch on the second step.

Next we proceeded to start following the second branch and all of its bifurcations. We found many other branches, but the shape of our diagram appeared to indicate that we were missing a pitchfork bifurcation. At the time we were using the non-symmetric code with $\beta = 0.001$ which could have caused the branch that seemed to be missing to be slightly separated from the other branches. We decided to go

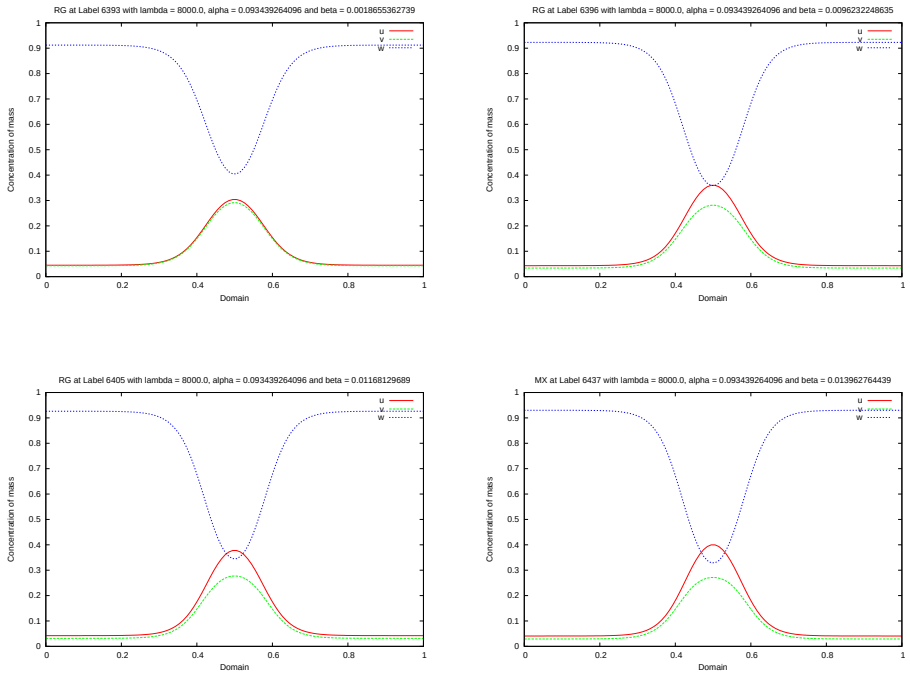


FIGURE 10. This figure depicts the change in droplet formation for the quadratic nonlinearity, as $\beta$ increases along the path in figure 5.

back to using the code with $\beta = 0$, which allowed us to find not only that branch, but several other branches out to $\lambda = 500$.

Finally we started trying to follow in $\alpha$ to get into the nucleation region. Beginning with $\lambda = 450$ we were able to follow back to $\alpha = 0.121$ from the branch with the lowest $L^2$ norm. This was in the nucleation region. We tried to trace back into the nucleation region at $\lambda = 450$ from a few of the other branches, but AUTO either started jumping between branches or simply intersected another branch and started moving away from the nucleation region.

On our one successful run into the nucleation region we obtained $\alpha = 0.121$ at four different points. We tried to vary in $\beta$ starting at each point. For the first three we only received end points from AUTO. We were able to follow the fourth

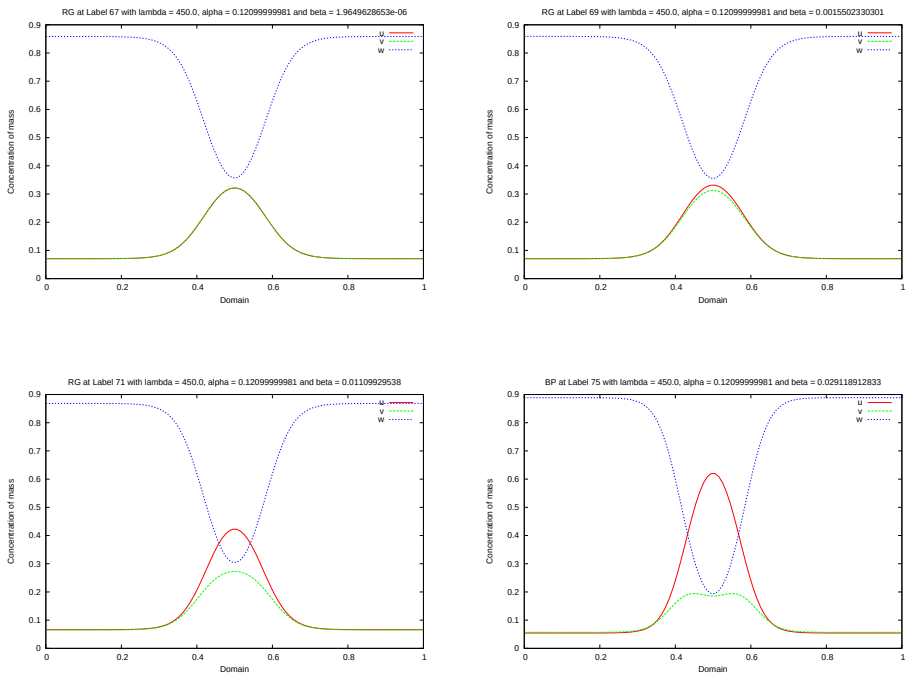


FIGURE 11. This figure depicts the change in droplet formation for the logarithmic nonlinearity, as $\beta$ increases along the path depicted in figure 5.

point with an $L^2$ norm of 0.1135 and $\beta = -0.06265$ briefly before AUTO started finding constant bifurcation points.

Figures 3, 4 and 5 compare and contrast the bifurcation diagrams resulting from the $\lambda$, $\alpha$ and $\beta$ runs respectively, for both nonlinearities. Interestingly, the diagrams depicting the $\alpha$ runs for both non-linearities are very different while the diagrams produced from the $\beta$ runs are almost identical. This suggests, at least qualitatively, that when in the spinodal region, the two nonlinearities behave very differently but once inside the nucleation region they behave more similarly. If similar results are obtained from future research then this would imply that from a materials science perspective, that the behavior of the Cahn-Morral system is not affected by the change in nonlinearity.

## 4. Future Work

We would like to successfully trace $\alpha$ back into the nucleation region from several branches at the same $\lambda$ value and compare droplet formations. We hope to eventually find which droplet formations are possible at each value of $\lambda$ for each nonlinearity. Our third partner James O'Beirne will be investigating a sixth degree polynomial nonlinearity and comparing the results with our investigations. Eventually the research should be expanded to two and three dimensions to see if results vary significantly. Also more than three components will be used. Both of these extensions, though requiring more computing power, will make the model considerably more reliable. We hope that future research will gather enough data to either disprove or support the assertion presented in this paper that the once inside the nucleation region, the system behaves identically, despite having different nonlinearities. Perhaps even a rigorous mathematical argument that explains the impact of changing nonlinearities.

## 5. Acknowledgements

The authors wish to thank Dr. Thomas Wanner, Dr. Evelyn Sander, James O'Beirne, the Department of Defense, the National Science Foundation, and the Department of Mathematical Sciences at George Mason University.

## References

[1] Kathleen T. Alligood, Tim D. Sauer, and James A. Yorke, *Chaos, An Introduction to Dynamical Systems*, Springer- Verlag New York, Inc., New York, New York, 1997.

[2] Jonathan P. Desi, Hanein H. Edrees, Joseph J. Price, Evelyn Sander, and Thomas Wanner, *The Dynamics of Nucleation in Stochastic Cahn-Morral Systems*, in preperation (2009).

[3] Junseok Kim and Kyungkeun Kang, *A numerical method for the ternary Cahn-Hilliard system with a degenerate mobility*, Applied Numerical Mathematics **59** (2009), 1029 – 1042.

[4] Stanislaus Maier-Paape, Barbara Stoth, and Thomas Wanner, *Spinodal Decomposition for Multicomponent Cahn-Hilliard Systems*, Journal of Statistical Physics **98** (1999), 871–895.

[5] Rüdiger Seydel, *From Equilibrium to Chaos*: *Practical Bifurcation and Stability Analysis*, Elsevier Science Publishing Co., Inc, 52 Vanderbilt Avenue, New York, New York, 1988.

Department of Mathematics, Virgina Tech

Department of Mathematics and Statistics, University of Maryland Baltimore County

*E-mail address*: cackerm@vt.edu

*E-mail address*: hardes1@umbc.edu